RESEARCH ARTICLE

Co-culture bioprinting of tissue-engineered bone-periosteum biphasic complex for repairing critical-sized skull defects in rabbits

Danyang Zhao¹†, Yu Wang²†, Zhencheng Yu¹, Chuandong Wang³, Hongbo Zhang⁴*, Dong Han¹*, Qingfeng Li¹*

¹Department of Plastic and Reconstructive Surgery, Shanghai Ninth People's Hospital, Shanghai Jiao Tong University School of Medicine, Shanghai, China

²Department of Cardiology, Shidong Hospital, Yangpu District, Shidong Hospital Affiliated to University of Shanghai for Science and Technology, Shanghai, China

³Department of Orthopedic Surgery, Xin Hua Hospital Affiliated to Shanghai Jiao Tong University School of Medicine, Shanghai, China

⁴School of Mechanical and Power Engineering, East China University of Science and Technology, Shanghai, China

(This article belongs to the *Special Issue: Novel Methods, Processes, and Materials of Bioprinting*)

†These authors contributed equally to this work.

*Corresponding author:
Qingfeng Li
(dr.liqingfeng@shsmu.edu.cn)
Dong Han
(handong12000@163.com)
Hongbo Zhang
(hbzhang@ecust.edu.cn)

Abstract

Tissue engineering based on bioprinting technology has broad prospects in the treatment of critical-sized bone defect. Nevertheless, it is challenging to construct composite tissues or organs with structural integrity. Periosteum and stem cells are important in bone regeneration, and it has been shown that co-culture engineering system could successfully repair bone defects. Here, a strategy of co-culture bioprinting was proposed, and a tissue-engineered bone-periosteum biphasic complex was designed. Poly-L-lactic acid/hydroxyapatite (PLLA/HA) was used to construct the supporting scaffold of bone phase. Gelatin methacryl (GelMA) loaded with rabbit bone mesenchymal stem cells (BMSCs) and periosteum-derived stem cells (PDSCs) were used to simulate the extracellular matrix and cellular components of bone and periosteum, respectively, and a co-culture layer was formed between the bone and the periosteum phase. By adjusting material ratios of PLLA/HA and crosslinking time of GelMA, a complex with good mechanical strength and cell activity was constructed and then implanted into the defect area of rabbit skull. The quantitative results of imaging and histology showed that the repair effect of bone-periosteum biphasic complex group was significantly better than that of other control groups, which demonstrated that the bone-periosteum biphasic complex was advantageous to both bone repair and regeneration. In general, using the co-culture bioprinting to construct engineered tissue is a very promising strategy, which is expected to be applied in the construction of more complex tissues and solid organs for tissue repair and organ transplantation.

Keywords: Bioprinting; Complex; Co-culture; Stem cells; Bone defect

1. Introduction

Critical-sized bone defects caused by trauma, infection, tumor, and developmental deformities are difficult to heal spontaneously[1]. The treatment of critical-sized bone defects still remains as a major challenge in plastic and reconstructive surgery, and the current clinical treatments, including bone grafts, distraction osteogenesis, and guided bone regeneration, often have limited effect[2].

Tissue engineering combined with scaffolds, stem cells, and growth factors to repair the bone defects could effectively solve the problems of tissue shortage and immune rejection caused by bone transplantation. With the development of new biomaterials, stem cell biology, and three-dimensional (3D) biological printing technology, tissue engineering has broad prospects in the treatment of bone defects. Good research progress has been reported by many studies devoted to the exploration of tissue-engineered bone construction strategies. However, the traditional tissue engineering technology is facing many problems, such as cell aging, difficulty in inducing differentiation, poor material properties, and bone reconstruction after absorption, which might not fulfill the requirements of large bone defect repair[3]. Three main components, which are considered important for bone tissue engineering, are osteoconductive scaffolds, osteogenic cells, and osteoinductive growth factors[4]. An osteoconductive scaffold can not only simulate the structure and function of extracellular matrix (ECM), but also provide effective mechanical support for adhesion, proliferation and differentiation of cells. As one of the main components of bone tissue, hydroxyapatite (HA), which has pores to allow tissue in-growth, has been used as a high-quality bone substitute[5]. All ceramic materials are brittle, but using biodegradable polymer–ceramic composites could improve biocompatibility and biomechanical properties[6]. Poly-L-lactic acid (PLLA) is a kind of biodegradable synthetic polymers that can be degraded to lactic acid through the metabolic pathway similar to the one in organisms. It has been safely used in the clinical application of soluble sutures, intra-bone implants, and soft tissue implants[7]. In our study, we mixed HA and PLLA to construct PLLA/HA scaffold, and then studied the effect of different molecular weights and mixing ratios on the mechanical strength. With the deepening research of stem cells, the study of stem cells-based regenerative medicine has drawn more public attention[8]. As one of the ideal seed cells, bone marrow mesenchymal stem cells (BMSCs) have been used in the treatment of various bone diseases[9]. Therefore, we applied BMSCs with osteogenic differentiation in the construction of tissue-engineered bone.

Periosteum, which covers the most part of the bone, plays a significant role in bone regeneration and homeostasis. Periosteum is not only a highly vascularized tissue, but also a reservoir of bone progenitor cells[10]. Due to the lack of periosteum, the repair effect of some bone grafts were poor, and the natural periosteum could be directly used for bone repair[11]. These remarkable effect of periosteum has led to extensive research on the use of periosteum-derived stem cells (PDSCs) for repairing critical-sized bone defect[12]. However, only a few studies have reported about tissue-engineered periosteum constructs[13,14]. In fact, both BMSCs and PDSCs are commonly used as the cell sources for bone tissue engineering. It has also been reported that co-culturing human BMSCs and PDSCs could produce synergistic effect on osteogenic differentiation[15]. Moreover, a growing number of studies have been focusing on using co-culture engineering system for effective repair of bone defect[16,17]. Here, we applied BMSCs and PDSCs to simulate the cellular components of bone and periosteum, respectively, and to construct tissue-engineered bone-periosteum biphasic complex on the basis of the co-culture mode, hoping to solve the problem of large bone defects from the perspective of physiological structure imitation.

Bioprinting is a 3D manufacturing technology for accurately distributing cell-loading biomaterials to construct complex living tissues and artificial organs. It has broad application prospects in the field of tissue engineering and regenerative medicine; however, it is challenging to construct tissues and organs with structural integrity using bioprinting[18,19]. Gelatin methacryl (GelMA) hydrogel, which has been widely applied in various biomedical situations, is similar to natural ECM and beneficial for the biological behavior of cells. Moreover, it can be crosslinked under ultraviolet (UV) light to form hydrogel with adjustable mechanical properties[20,21]. We intended to take advantages of bioprinting in mechanics, structure, and personalization, and a novel strategy of co-culture bioprinting was proposed. GelMA loaded with BMSCs and PDSCs was used to simulate the ECM and cell components of bone and periosteum phase, respectively. The bone-periosteum biphasic complex was constructed by combining PLLA/HA supporting scaffold, and the repair effect was evaluated from the perspective of imaging and histology after repairing the critical-sized calvarial defect of rabbit.

In summary, we designed and used the multinozzle distribution modules of 3D bioprinter system to deposit different cells-laden GelMA together with biosynthetic PLLA/HA scaffold to construct a tissue-engineered bone-periosteum biphasic complex, and then evaluated the characteristics and functions of the constructed complex both *in vitro* and *in vivo*. Through this work, we hope to

clarify the advantages and prospects of co-culture bioprinting in the construction of complex living tissues and organs, and to promote the clinical translational research of composite biomaterials, stem cell differentiation, and bioprinting.

2. Materials and methods

2.1. Cell culture and co-culture

2.1.1. Culture of BMSCs and PDSCs of rabbit

BMSCs of rabbit (rabBMSCs) were acquired according to our previous study[22]. Briefly, bone marrow blood of New Zealand White rabbit was extracted from the iliac bone, and then cultured in high-glucose Dulbecco's modified eagle's medium (DMEM; Hyclone, USA) with 10% fetal bovine serum (FBS; Gibco, USA), 100 U/mL penicillin, and 100 µg/mL streptomycin (Hyclone, USA). PDSCs of rabbit (RabPDSCs) were obtained by enzymatic digestion as previously described[12,23]. In brief, the periosteum of rabbit skull was carefully harvested and digested by 0.25% type I collagenase (Sigma, USA). The digested suspension was then filtered through a 70 µm nylon mesh, and then centrifuged at 1,500 rpm. The cells were resuspended in complete F-12 DMEM supplemented with 10% FBS, 100 U/mL penicillin, and 100 µg/mL streptomycin for culturing. Cells from the third to fifth generations were used.

2.1.2. Multidirectional differentiation of rabBMSCs and rabPDSCs

The primary cells were identified by muitidirectional differentiation. Alkaline phosphatase (ALP) staining was used to analyze osteogenic differentiation after 7 days of induction. Alizarin red S staining was used to detect the mineralized nodules after 3 weeks. For adipogenic differentiation, the newly produced lipid vacuoles could be confirmed by oil red O staining after 12 days. For chondrogenic differentiation, the cells that have been induced for 3 weeks were detected by Alcian blue staining.

2.1.3. Real-time polymerase chain reaction (qPCR)

Total RNA was extracted form rabBMSCs and rabPSDCs using Trizol reagent (Invitrogen, USA) after 7 days of osteogenic differentiation. After the reverse transcription reaction, real-time polymerase chain reaction (qPCR) was performed with a QuantStudio 6Flex system (Life Technologies, USA) using SYBR Premix (Takara, Japan). The primer sequences used in this study were described as follows: collagen I (COL1) – 5'-CAGCGGCTCCCCATTTTCTA-3' (forward), 5'-ATCTCAGCTCGCATAGCACC-3' (reverse); osteocalcin (OCN) – 5'-AGAGTCTGGCAGAGGCTCA-3' (forward), 5'-CAGGGGATCCGGGTAAGGA-3' (reverse); osteopontin (OPN) – 5'-AGCGTGGAAACCCAAAGTCA-3' (forward), 5'-GCTCGATGGCTAGCTTGTCT-3' (reverse); runt-related transcription factor 2 (RUNX2) – 5'-GATGACGTCCCCGTCCATTC-3' (forward),

5'-GGAACAGGGTGGTGGAAGAC-3' (reverse); glyceraldehyde phosphate dehydrogenase (GAPDH) – 5'-AGACACGATGGTGAAGGTCG-3' (forward), 5'-TGCCGTGGGTGGAATCATAC-3' (reverse). The qPCR program was as follows: denaturation at 95°C for 10 s, and 40 cycles at 95°C for 10 s, and 60°C for 30 s. The results were analyzed using the comparison CT ($2^{-\Delta\Delta Ct}$) method. GAPDH was used as an internal control, and each sample was analyzed in triplicate.

2.1.4. Co-culture of rabBMSCs and rabPDSCs

We co-cultured rabBMSCs and rabPDSCs using 0.4 µm polycarbonate membrane transwell insert (Corning, USA). In this experiment, three groups of cells were used: (I) rabBMSCs, (II) rabPDSCs, and (III) rabBMSCs+rabPDSCs. In group (III), rabPDSCs were seeded onto the upper layer of the chamber. After culturing for 24 h, osteogenic induction medium was replaced, while the cells of the control group were still cultured in complete DMEM.

2.2. 3D extrusion-based bioprinting

2.2.1. Materials preparation

The raw material of PLLA with molecular weights of 32,000 (3.2 W) and 54,000 (5.4 W) were purchased from Daigang Inc (Shandong, China). HA (>97%, MW = 502.31) was purchased from Kingmorn Inc (Shanghai, China). Gelatin of porcine skin was obtained from Sigma-Aldrich (New Jersey, America). I-2959 (>98.0%, MW = 224.26), the photoinitiator, was purchased from TCI (Shanghai, China). Methacrylic anhydride (MA) and dichloromethane (≥99.5%, MW = 84.93) were purchased from General Reagent of Titan Inc (Shanghai, China).

PLLA/HA composites with different ratios were prepared. Briefly, PLLA was dissolved in dichloromethane to form a transparent colloidal solution. HA powder was then added to the PLLA solution at mass fraction of 10%, 20%, and 30%. The synthesis of GelMA has been reported previously[24]. Briefly, gelatin was dissolved in phosphate-buffered saline (PBS, 10% (w/v)), and then MA was added (20% v/v). The fully mixed solution was then reacted at 50°C for 3 h, and then dialyzed with distilled water for 1 week. Finally, the GelMA precursor could be obtained by freeze-drying and stored for further use.

The precursor of GelMA and I-2959 were dissolved in PBS (5% (w/v) hydrogel solution with 0.1% (w/v) photoinitiator). Next, rabBMSCs and rabPDSCs were mixed with the prepared hydrogel at a density of 5×10^6/mL. The prepared bioink was rewarmed before being added to the printing cartridges.

2.2.2. 3D bioprinting process

The 3D Bioplotter printer (Envision Tec, Germany) was applied to construct the complex structure. One of the
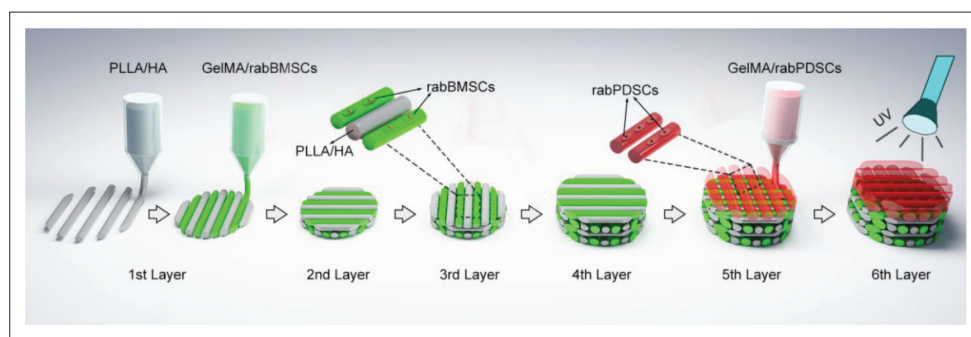
Figure 1. Diagram of the bioprinting process of bone-periosteum biphasic complex. Overall, the complex was designed as a flat cylinder structure with six layers, and three cartridges were used to deliver poly-L-lactic acid/hydroxyapatite (PLLA/HA) complex, bone marrow mesenchymal stem cells of rabbit (rabBMSCs)-loaded gelatin methacryl (GelMA) and periosteum-derived stem cells of rabbit (rabPDSCs)-loaded GelMA, respectively. First, the lower four layers of bone phase structure were printed. Each layer was alternately printed by PLLA/HA composite and rabBMSCs-laden GelMA. Next, the upper two layers of periosteum phase were printed, which consisted of rabPDSCs-laden GelMA. After printing all six layers, the bone-periosteum biphasic complex was finally crosslinked with 365 nm UV light.

high-temperature cartridges was used to print PLLA/HA scaffold, and the other two low-temperature cartridges were used to print rabBMSCs-laden and rabPDSCs-laden GelMA, respectively. A printing model in stereolithography file format was created and sliced, and then specific printing parameters were adjusted. Samples were printed directly in the dishes, and all printing processes were carried out in a sterile environment.

The bone-periosteum biphasic complex was designed as a flat cylinder with six layers. The flow process diagram is shown in Figure 1. The lower four layers were bone phase with 1.6 mm line spacing, consisting of PLLA/HA composite and rabBMSCs-laden GelMA. The upper two layers were periosteum phase with 1.2 mm line spacing, which was just composed of rabPDSCs-laden GelMA. A co-culture layer was formed between the bone phase and the periosteum phase. The samples were crosslinked with 365 nm UV light after printing and then incubated in the culture medium for 1 week.

2.3. Characterization of PLLA/HA scaffolds
2.3.1. Mechanical test
We applied the Instron Testing Machine (PA, USA) to test the mechanics of different PLLA/HA scaffolds. According to the molecular weight of PLLA and mass fraction of HA, six kinds of different PLLA/HA scaffolds were printed. Compression tests were carried out, the stress–strain curves were recorded, and the values of maximal force and elastic modulus were obtained.

2.3.2. Cell viability
1×10^6 rabBMSCs were seeded on 5.4 W PLLA/20% HA scaffolds and then cultured in 24-well plates (1 mL/well). The cell proliferation was detected by cell counting kit-8 (CCK-8; Dojindo, Japan) assay within 2 weeks. Briefly, the analytical solution was added and incubated, and the

absorbance value was then measured with the microplate reader (Tecan, Switzerland).

2.3.3. Scanning electron microscope
The micro morphology of scaffold and cell proliferation on its surface were observed with the use of scanning electron microscope (SEM; FEI Quanta 250, USA). The rabBMSCs were cultured on the PLLA/HA scaffolds for 1 week, fixed with 2.5% glutaraldehyde, dehydrated, dried and then sprayed with gold for observation.

2.4. Characterization of GelMA bioinks
2.4.1. Physical properties of GelMA
The rheological property of GelMA was measured by the HAAKE MARS III rheometer (Thermo Fisher, USA) at room temperature, and the Fourier transform infrared spectroscopy (FTIR) spectra of the GelMA was obtained using a FTIR spectrophotometer (Bruker, Vertex 70). To study the degradation rate of GelMA, the samples were immersed in PBS containing 10 μg/mL lysozyme and incubated at 37°C. The enzyme solution was replaced every 3 days. The percentage of weight loss (%) was determined by the Equation I:

$$\text{Weight loss}\left(\%\right) = \frac{wi - wf}{wi} \times 100\% \tag{I}$$

where wi is the initial dry weight of the construct and wf is the final dry weight during 14 days of incubation.

2.4.2. Living and dead cell staining
The 3D-printed structures were crosslinked with UV light irradiation for 30, 45, and 60 s. Live/dead viability/cytotoxicity kit (Invitrogen, USA) was used to detect the activity of cells on the 3D-printed scaffold. Briefly, working solutions were directly added to rabPDSCs-laden and rabBMSCs-laden GelMA, and then incubated. Fluorescence microscopy (Nikon, Japan) was applied to

evaluate the staining of cells. Live cells were shown in green, and dead cells were in red. The cell viability was calculated as the ratio of the number of live cells to total cells.

2.4.3. Laser confocal microscope
RabBMSCs and rabPDSCs were labeled with two fluorescent dyes (Invitrogen, USA), namely DiO (green) and DiI (red). A laser scanning microscope (Zeiss, Germany) was used to analyze the distribution of fluorescent labeled cells in the printed structure.

2.5. Calvarial bone reconstruction
2.5.1. Repair of critical-sized skull defect in rabbits
Fifteen male New Zealand White rabbits (2–2.5 kg) were divided into five groups (n = 6): (I) blank, (II) PLLA/HA, (III) PLLA/HA+GelMA, (IV) PLLA/HA+GelMA+rabBMSCs, and (V) PLLA/HA+GelMA+rabBMSCs+rabPDSCs. Rabbits were anesthetized and the calvarium were exposed. Two symmetrical 8 mm-diameter hole-shaped bone defects were established along the midline of the *sutura cranii* with a circular drill. In group (I), the defect area was retained without repair. In group (II), the defect area was repaired with PLLA/HA scaffold alone. In group (III), PLLA/HA with GelMA to repair the defect area. In group (IV), bone-phase combined with scaffold was implanted in the defect area. In group (V), bone-periosteum biphasic complex was implanted in the defect area. All rabbits were sacrificed after 12 weeks, and the skulls were fixed with 4% paraformaldehyde.

2.5.2. Micro-computed tomography (μCT)
All samples were imaged with high-resolution micro-computed tomography (μCT) imaging system (Scanco μCT 100, Switzerland). The bone tissue was separated, and the defect area was reconstructed. Finally, the regenerated bone volume (BV), bone volume/total volume (BV/TV), trabecular number (Tb. N), trabecular thickness (Tb. Th), and trabecular spacing (Tb. Sp) in the bone defect area were measured and statistically analyzed.

2.5.3. Histological staining
The skull specimens were decalcified for 2 months. After dehydration with graded alcohol, the skulls in the defect area were embedded in paraffin and cut into 7 μm-thick slices along the coronal axis. Hematoxylin and eosin (H&E), Masson's trichrome and immunohistochemical (IHC) staining of osteocalcin (OCN) were conducted to evaluate the newly formed bone within the defect area. Image J software was applied to conduct quantitative analysis of collagen volume fraction and mean density of OCN (%). The collagen volume fraction is equal to the ratio of collagen area to total tissue area, and the mean density of OCN (%) represents the proportion of positive expression of OCN in tissue.

2.6. Statistical analysis
The statistical results are expressed as mean ± standard deviation. Student's *t*-test and one-way analysis of variance (ANOVA) were used to analyze the differences of data. $P <$ 0.05 was considered statistically significant.

3. Results
3.1. Co-culture of rabBMSCs and rabPDSCs promoted osteogenic differentiation *in vitro*
In order to obtain seed cells of the tissue-engineered bone-periosteum biphasic complex, rabBMSCs and rabPDSCs were isolated. It was found that the cells were spindle-shaped fibroblasts, which grew and proliferated rapidly *in vitro* (Figure 2A and F). Multidirectional differentiation of the two sets of seed cells were induced *in vitro*. ALP staining showed that the staining of cells in osteogenic group was positive (Figure 2B and G). Alizarin red S staining showed calcium nodule deposition (Figure 2C and H), oil red O staining displayed lipid droplet formation (Figure 2D and I), and Alcian blue staining resulted in the formation of blue acid polysaccharide in the induction group (Figure 2E and J). Besides, we detected the expression of some osteogenesis-related genes in rabBMSCs and rabPDSCs using qRCR after seven days of osteogenesis induction. As shown in **Figure S1**, the expression of COL1, OCN, OPN, and RUNX2 in rabBMSCs and rabPDSCs increased significantly after osteogenesis induction, which was significantly different from the control group. These above results illustrated that rabBMSCs and rabPDSCs had multidirectional differentiation ability, which was in accordance with the characteristics of stem cells. RabBMSCs and rabPDSCs were then co-cultured in transwell chambers. The results of ALP staining and Alizarin red S staining of the co-cultured cells and their osteogenic differentiation groups were significantly different from those of the control group, indicating that co-culturing of rabBMSCs and rabPDSCs could promote osteogenic differentiation *in vitro* (Figure 2K and L).

3.2. Characterization of PLLA/HA scaffolds
Bone scaffold should not only be able to bear certain mechanical stress, but also have good biocompatibility in the process of *in vivo* repair. First, we applied synthetic polymer–ceramic composites to construct 3D-printed PLLA/HA tissue-engineered bone scaffolds by mixing PLLA of 3.2 W and 5.4 W with HA of 10%, 20%, and 30% mass fractions, respectively, and then explored the effect of different mixing ratios on the mechanical strength of the scaffolds (Figure 3A). The results showed that when the mass fraction of HA was 20%, the maximal force was higher than that of 10% and 30% groups, and the maximal force of HA of 20% and 30% mass fraction groups were significantly
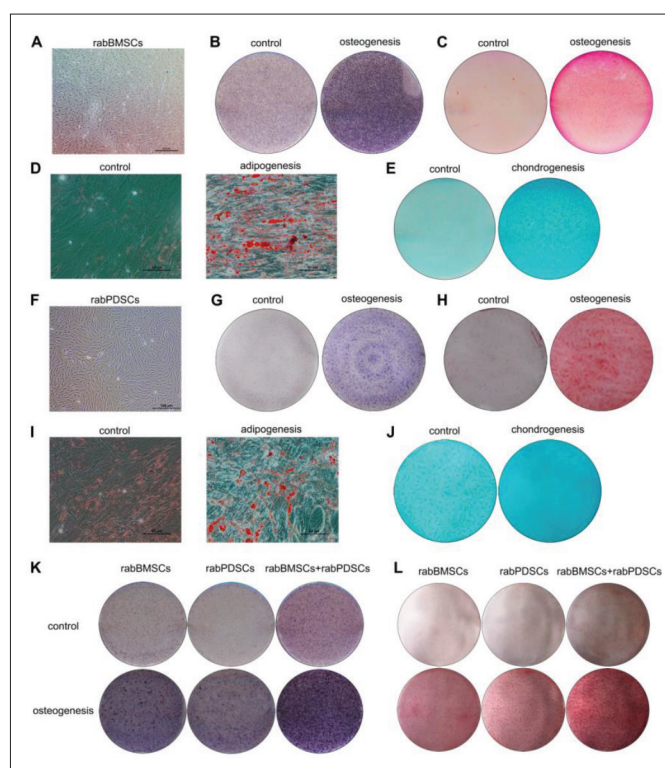
Figure 2. Cell culture and co-culture of rabBMSCs/rabPDSCs. (A) The morphology of rabBMSCs (scale bar = 200 μm). (B) The alkaline phosphatase (ALP) staining of rabBMSCs after 1 week of osteogenic induction. (C) The Alizarin red S staining of rabBMSCs after 3 weeks of osteogenic differentiation. (D) The oil red O staining of rabBMSCs after 12 days of adipogenic differentiation (scale bar = 50 μm). (E) The Alcian blue staining of rabBMSCs after 3 weeks of chondrogenic differentiation. (F) The morphology of rabPDSCs (scale bar = 200 μm). (G) The ALP staining of rabPDSCs after 1 week of osteogenic induction. (H) The Alizarin red S staining of rabPDSCs after 3 weeks of osteogenic differentiation. (I) The oil red O staining of rabPDSCs after 12 days of adipogenic differentiation (scale bar = 50 μm). (J) The Alcian blue staining of rabPDSCs after 3 weeks of chondrogenic differentiation. (K) The ALP staining of rabBMSCs and rabPDSCs, co-culturing of rabBMSCs and rabPDSCs, as well as their osteogenic induction groups after 1 week. (L) The Alizarin red S staining of rabBMSCs and rabPDSCs, co-culturing of rabBMSCs and rabPDSCs, as well as their osteogenic induction groups after 3 weeks.

higher than that of 10% mass fraction group (Figure 3B). In addition, the elastic modulus of 5.4 W PLLA/20% HA group was the highest, which was significantly different from that of 5.4 W PLLA/10% HA group. Therefore, in the subsequent printing process, we adopted the mixed proportion of 5.4 W PLLA with 20% HA to construct the bone supporting scaffold of the biphasic complex.

Then, we analyzed the biocompatibility of PLLA/HA scaffold through CCK-8 experiment and tested the proliferation of rabBMSCs on the 3D-printed scaffolds. The results showed that the number of cells increased continuously within 14 days (Figure 3C). Moreover, as shown by SEM, PLLA/HA scaffold showed staggered porous channels, while rabBMSCs could adhere and stretch on the surface of the scaffold with extended pseudopodia (Figure 3D).

3.3. 3D bioprinting cells pattern
In the process of 3D bioprinting, the rheological property of GelMA plays a key role in forming a stable 3D structure.

The storage modulus (G') of GelMA was shown in the **Figure S2A**. It could be seen that under UV irradiation, the storage modulus (G') of GelMA increased rapidly, while the dissipation modulus (G") was hardly changed. GelMA reached the gelation conversion point after 20 s, which indicated that the hydrogel needs at least 20 s of UV irradiation to complete the crosslinking. After 20 s, the G' of GelMA continuously improved with the extension of UV irradiation time, indicating that the strength of the hydrogel was getting better. **Figure S2B** shows the FTIR spectra of GelMA. There was a characteristic absorption peak assigned to peptide bond, in which the amide I appearing in the range 1630–1690 cm^{-1} is mainly related to C=O stretching. The degradation curve showed that GelMA was rapidly degraded under the action of lysozyme, and it was almost completely degraded on the 14th day (**Figure S2C**).

In our study, GelMA was used to load rabPDSCs and rabBMSCs to simulate the periosteum phase and bone phase of the biphasic complex, respectively. As shown in
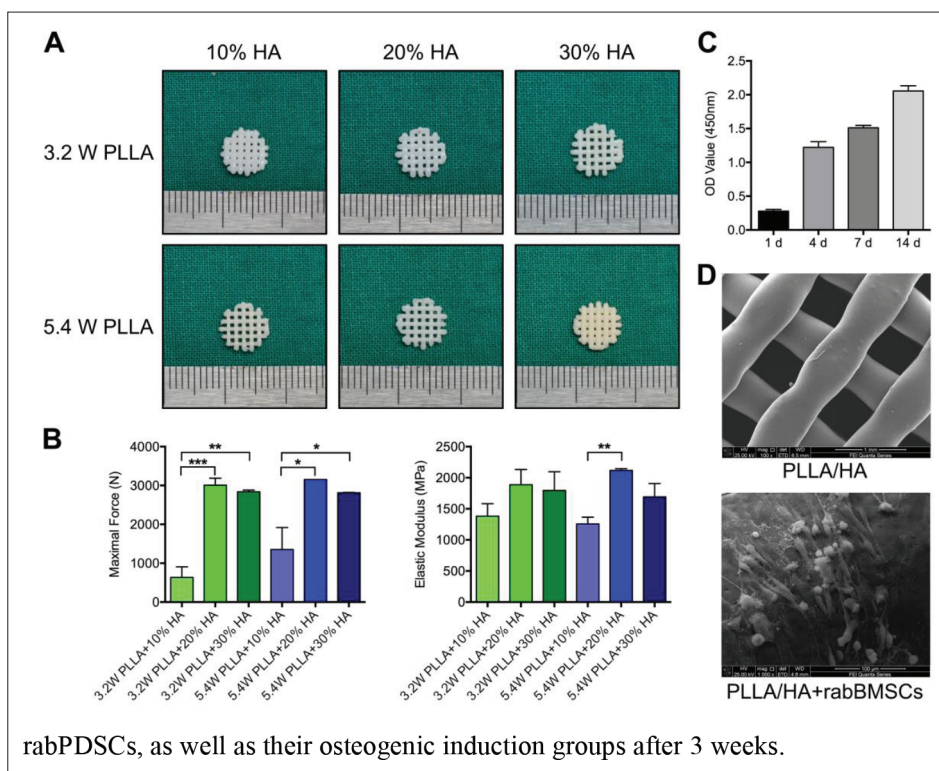
Figure 3. Characterization of PLLA/HA scaffolds. (A) The images of 3D-printed PLLA/HA scaffolds produced by mixing PLLA (3.2 W and 5.4 W molecular weight) and HA (10%, 20%, and 30% mass fraction) (scale bar = 1 mm). (B) Maximal force and elastic modulus of different PLLA/HA scaffolds. (C) Proliferation of rabBMSCs on PLLA/HA scaffold. (D) Microstructure and biocompatibility of PLLA/HA scaffold by scanning electron microscope (SEM) (scale bar = 1 mm for PLLA/HA; scale bar = 100 μm for PLLA/HA+rabBMSCs). Each bar represents mean ± standard deviation. *$P < 0.05$; **$P < 0.01$; ***$P < 0.001$.

Figure 4A, periosteum phase and bone phase were round structures, and the materials between the two layers were printed vertically. The line spacing of the upper layer was 1.2 mm, while the line spacing of the lower layer was 1.6 mm. On the right of Figure 4A were the instant photographic images after bioprinting. The cells were spherical and evenly distributed in the hydrogel under the light microscope (Figure 4B). Since the crosslinking of GelMA by UV light would affect the cell activity, we applied different time durations to crosslink GelMA, and then stained the cells to distinguish living and dead cells. The fluorescent images showed that the number of dead cells grew with the increase of crosslinking time, especially on the surface of the hydrogel (Figure 4C). GelMA with different crosslinking durations were then cultured in the medium. The results showed that the activity of cells in GelMA with prolonged UV crosslinking was lower than that of short-term UV crosslinking. However, the cell viability in GelMA after UV crosslinking of 30 s and 45 s was higher than 75% after 7 days (Figure 4D). Furthermore, as shown by the CCK8 experimental results, both of rabPDSCs and rabBMSCs in GelMA continued to proliferate within 14 days of culture *in vitro* (Figure 4E).

RabPDSCs and rabBMSCs were labeled with DiI (red) and DiO (green) fluorescent dyes, respectively, and the 3D structure was constructed. The 2D and 3D fluorescent images could clearly show the hierarchical structure and the co-culture bioprinting pattern of the two types of cells (Figure 4F).

3.4. Calvarial bone reconstruction of rabbits
In order to study the osteogenic and repair effect of the complex *in vivo*, treatment was performed on the skull defect area in the rabbits of the five groups (Figure 5A). Images of μCT scanning showed that relatively complete bone tissue was formed in the defect area of composite implant groups, while the untreated group and the PLLA/HA group showed only a little bone tissue growing inward from the edge and mainly confined around the implant. The new bone in the defect area was reconstructed and quantified, as shown in Figure 5B, with the improved complexity of the scaffold, the BV, BV/TV, and Tb. N of the reconstructed new bone were gradually increased, and the Tb. N in group (V) was significantly different from that of group (III). There was no significant difference of the Tb. Th among five groups; however, the Tb. Sp decreased
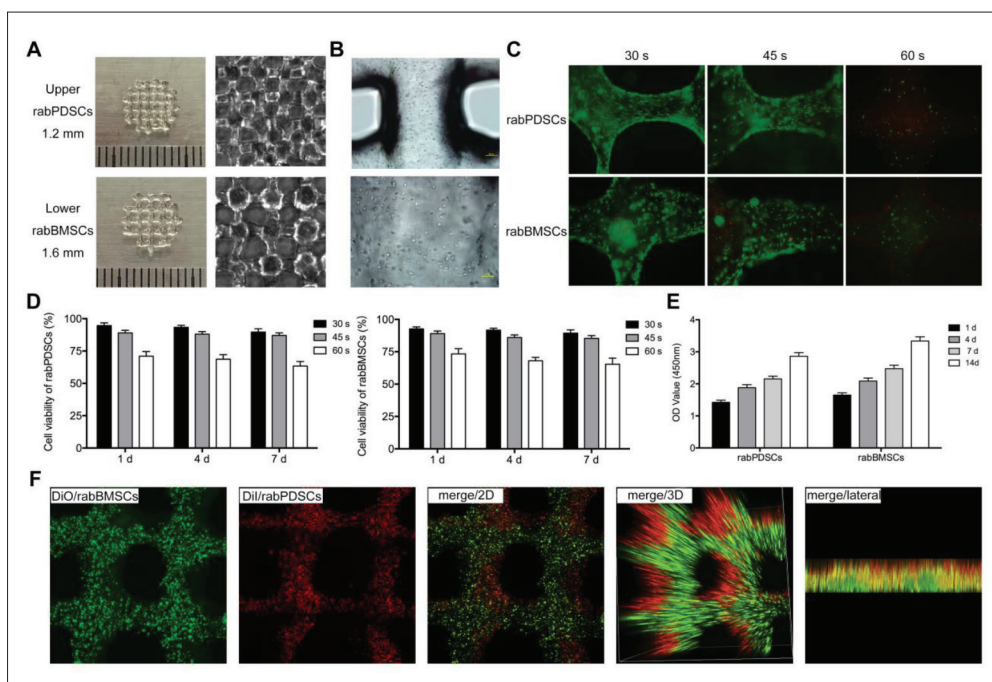
Figure 4. Three-dimensional (3D) patterning of cells bioprinting. (A) The photographs of 3D-printed GelMA loaded with rabPDSCs and rabBMSCs (scale bar = 1 mm). (B) The morphology of rabPDSCs and rabBMSCs in GelMA (scale bar = 100 μm for upper rabPDSCs; scale bar = 60 μm for lower rabPDSCs). (C) Living and dead cell staining of rabPDSCs and rabBMSCs in GelMA after crosslinking with UV light for 30, 45, and 60 s. (D) Cell viability of rabPDSCs and rabBMSCs in GelMA after crosslinking with UV light for 30, 45, and 60 s on days 1, 4, and 7, respectively. (E) Proliferation of rabPDSCs and rabBMSCs in GelMA after crosslinking with UV light for 45 s after 1, 4, 7, and 14 days. (F) Fluorescent image of the 3D-printed rabBMSCs-loaded GelMA and the rabPDSCs-loaded GelMA. Each bar represents mean ± standard deviation. $*P < 0.05$; $**P < 0.01$; $***P < 0.001$.
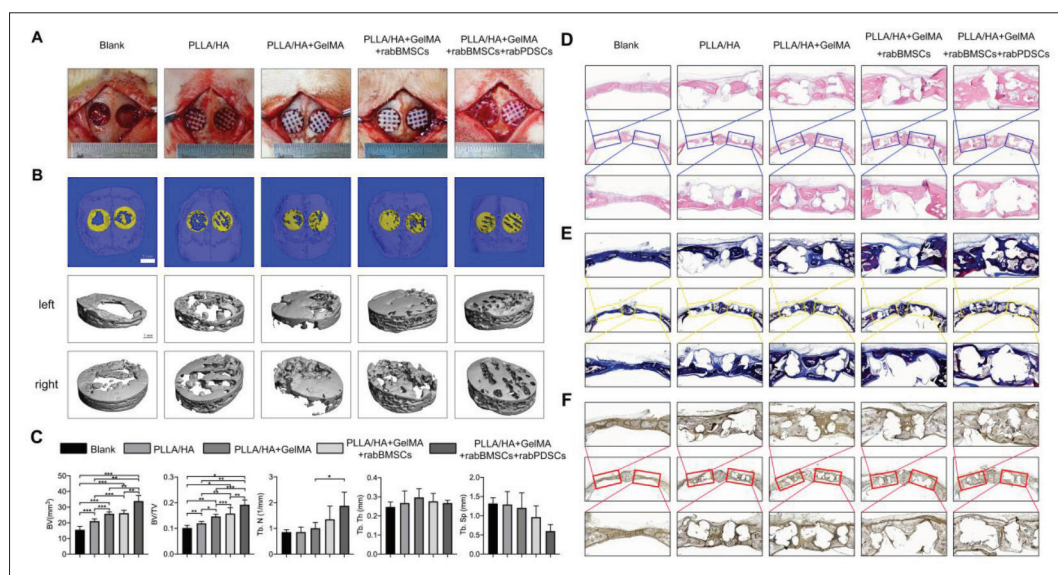

Figure 5. Calvarial bone reconstruction. (A) Five groups of postoperative photos of the repair of rabbit skull defect (scale bar = 0.5 mm). (B) Representative micro-computed tomography (μCT) scanning and reconstructed images of rabbit skull in five groups after 12 weeks (scale bar = 5 mm for scanning images; scale bar = 1 mm for reconstructed images). (C) The quantitative results of bone volume (BV), bone volume/total volume (BV/TV), trabecular number (Tb. N), trabecular thickness (Tb. Th), and trabecular spacing (Tb. Sp) in the bone defect area of five groups. (D) Hematoxylin and eosin (H&E) staining of rabbit skull and the newly formed bone within the defect area (scale bar = 1000 μm). (E) Masson's trichrome staining of rabbit skull and the newly formed bone within the defect area (scale bar = 1000 μm). (F) Immunohistochemical (IHC) staining of osteocalcin (OCN) of rabbit skull and the newly formed bone within the defect area (scale bar = 1000 μm). The areas selected in blue, yellow, and red boxes are defect areas (scale bar = 200 μm). Each bar represents mean ± standard deviation. $*P < 0.05$; $**P < 0.01$; $***P < 0.001$.

gradually from group (I) to group (V) (Figure 5C). To sum up, the µCT results showed that using bone-periosteum biphasic complex to repair bone defects was better than other control groups.

We also applied H&E, Masson's trichrome and IHC staining of OCN to evaluate the maturity of the newly formed bone. H&E staining showed that there was new bone in the skull defects. With the increasing complexity of the scaffold, the fibrous tissue decreased relatively, while the mature bone tissue increased gradually (Figure 5D). Masson's trichrome staining showed that the newly formed osteoid tissue was blue, and the boundaries between the new bone and the edge of skull defect became blurred in the composite repair groups (Figure 5E). IHC staining of OCN could also be used to evaluate osteogenesis. As shown in Figure 5F, both original cortical bone and newly formed bone expressed OCN. Based on the quantitative results of collagen volume fraction and mean density of OCN (%), the content of collagen and the expression of OCN from group I to group V were increasing, respectively, indicating the improved quality of bone formation as evidenced by the formation of new bone, which was more mature (**Figure S3**). Taken together, bone-periosteum biphasic complex is advantageous to bone repair and regeneration.

4. Discussion

To date, tissue-engineered bone has been used in the treatment of bone defects and other bone diseases, but there were relatively few clinical reports[25]. In order to improve the repair of bone defects, especially of the critical-sized bone defects, studies on periosteum tissue engineering have been conducted. Various bionic artificial periosteum, including cell-sheet artificial periosteum, acellular scaffold artificial periosteum and synthetic scaffold artificial periosteum, have been developed. As a direct substitute of natural periosteum, the tissue-engineered periosteum could significantly improve the efficiency of bone transplantation and scaffold engineering[26]. However, most studies separated the structure of bone and periosteum and only constructed the tissue-engineered periosteum structure. The highlight of our study is to treat the bone and periosteum structure as a whole, and attempt to improve bone regeneration in morphology and function at the same time. On the one hand, we promoted osteogenic differentiation of stem cells through co-culture strategy, and then used bioprinting technology to build complex structure. The results of our study showed that the 3D bioprinting tissue-engineered bone-periosteum biphasic complex had good mechanical strength and cell activity, and also achieved good repair effect after being implanted into the skull defect area of rabbit.

Bone healing depends on osteogenesis, osteoinduction, and osteoconduction indispensably and simultaneously[27,28]. In the process of bone healing, mesenchymal stem cells, including those in bone marrow and periosteum, provide bone progenitor cells that differentiate into osteoblasts; moreover, osteoinductive factors can accelerate this process[29]. In our study, we used rabBMSCs and rabPDSCs to simulate the cell components of bone phase and periosteum phase within the complex structure. As shown in Figure 2, rabBMSCs and rabPDSCs had the ability to differentiate into osteoblasts, adipocytes, and chondrocytes. In addition, co-culture of these two cells could significantly promote the osteogenic differentiation. In fact, the successful application of BMSCs in bone tissue engineering also lies in its ability to secrete inductive factors, including vascular endothelial growth factor (VEGF)[30]. Other studies have reported that the osteogenic and angiogenic factors of PDSCs increased under mechanical stimulation[31,32]. Furthermore, bone healing process also depends on a sufficient of blood vessels. Studies have shown that avascularity is the main factor in the pathogenesis of critical-sized bone defects[33]. Osteoinductive factors, including pro-inflammatory cytokines, growth factors, and angiogenic factors, are transmitted to the fracture site through the vascular system[4]. Chen *et al.* reported that neovascularization was also found after the co-culturing of bone marrow and periosteal mesenchymal stem cells[15]. Therefore, in this study, we planned to evaluate the angiogenic factors within the complex, and even improved the construction of the complex by introducing the vascular structural system in the future. Due to the complexity of bone tissue structure, the macro and micro structures of the composite need to be further optimized, and the angiogenesis mechanism also needs to be further clarified to improve the performance of tissue-engineered complex.

Bone conductive scaffold is necessary to allow bone to grow onto its surfaces[34]. Combining the advantages of synthetic polymers and ceramic materials, we mixed PLLA and HA in a certain proportion and found an interesting phenomenon that the mechanical strength of different scaffolds did not increase with the increasing of the mixing proportion of materials (Figure 3A and B). During the printing process, when the molecular weight of PLLA and the mass fraction of HA in the mixed materials gradually increased, higher melting temperature was required to make them printable. Polymer–ceramic materials are printed by fused deposition modeling, and different melting temperatures often affect the mechanical properties of the composites[35]. Therefore, we should not only consider the biocompatibility of materials, but also think about the impact of printing mode on the properties of materials in the process of bioprinting, which would

directly affect the scaffold conductivity. As a superior polymer–ceramic composite, PLLA/HA has been widely studied and applied in various aspects of biomedicine[6,36]. Although the degradation products of PLLA may cause inflammatory reaction, the subclinical inflammation of the host could effectively promote collagen synthesis[7]. When the ceramic is combined with PLLA matrix composites, its biocompatibility can also be improved. Besides, PLLA/HA composites could effectively solve the problems caused by metal implants, such as stress shielding and the need for a second operation[37]. Our study found that 5.4 W PLLA+20% HA scaffold was not only superior to other material groups in maximum force and elastic modulus, but also had good biocompatibility. For the critical-sized bone defect, the ideal tissue engineering structure should provide an appropriate environment similar to the natural healing. The mechanical strength and bone conduction properties of the scaffolds are required to be higher for the long and irregular bone defects at the stressed sites. Such a graft should have sufficient strength to promote not only the integration with the host tissue, but also the load transfer under load-bearing conditions. In our study, a rabbit skull defect model was used to validate the co-culture bioprinting mode *in vivo*. The bone defect at the weight-bearing site should also be investigated, and it is necessary to select alternative materials with better mechanical strength. After optimizing the printing structure and design, we could repair the segmental defect of long bone in other larger animals. In addition to animal species, appropriate age and size of bone defect should also be considered[38].

GelMA-based hydrogels have suitable biological and adjustable physical properties[20]. From the processing point of view, GelMA can be crosslinked under UV light to achieve adjustable mechanical properties. It can also be micromanufactured using different methods to generate personalized structures[20]. GelMA applied in bioprinting is a tissue repair strategy based on cell-laden GelMA transplantation. The combination of GelMA and cells play a key role in this process[39]. GelMA-based hydrogels are very similar to ECM in some basic characteristics, there are cell attachment that allow cells to proliferate and diffuse in them[20]. In our study, GelMA showed good wrapping and biological activity. By exploring the effect of different crosslinking durations on cell activity, we found that rabBMSCs and rabPDSCs in GelMA still showed high cell viability and proliferation activity after crosslinking (Figure 4B–E). Importantly, after crosslinking, the 3D co-culture mode of rabBMSCs and rabPDSCs was successfully realized within GelMA (Figure 4F). In fact, the physical properties of GelMA hydrogels could be adjusted by a series of parameters, such as material and initiator concentration, as well as the UV exposure time[40]. Therefore, we need to further explore the above parameters and adjust the mechanical properties of GelMA accordingly.

To sum up, by forming a co-culture layer between the bone phase and periosteum phase, the new co-culture bioprinting strategy could not only simulate the normal bone-periosteum tissue in structure, but also significantly improve the repair effect compared with other monophasic scaffolds, thereby illustrating the advantages and prospects of this bioprinting strategy in constructing complex living tissues and organs. Thus, the technology of 3D bioprinting could meet the requirements for establishing an integrated co-culture system, and the combination of co-culture concept and engineering tissue construction could be considered a promising strategy for repairing critical-sized bone defects. However, there are some limitations in this study. First, it is difficult to control the osteogenic differentiation direction of stem cells *in vivo*. Second, the degradation and absorption of materials and the rate of bone reconstruction *in vivo* also need to be matched. In addition, the structural design and construction of the complex rely on the advances of bioprinting technology.

5. Conclusion

In this study, the strategy of co-culture was introduced into the 3D bioprinting system to manufacture tissue-engineered bone-periosteum complex and improve bone defect repair ability. The structure of natural bone tissue consisting of periosteum phase and bone tissue phase was physiologically imitated, and a co-culture layer was formed between these two different phases. To the best of our knowledge, this is the first study describing the application of bioprinting to construct bone-periosteum complex. Through optimizing the parameters of material ratio of bone scaffold and crosslinking time of GelMA, an integrated bionic structure was constructed and a good repair effect was achieved. The results showed that the 3D bioprinting tissue engineering structure based on co-culture system might solve the problem of critical-sized bone defect, and was expected to construct other complex tissues and organs.

Conflict of interest

The authors declare no conflicts of interests.

Author contributions

Conceptualization: Qingfeng Li, Danyang Zhao, Yu Wang
Formal analysis: Zhencheng Yu, Chuandong Wang
Investigation: Danyang Zhao, Yu Wang, Zhencheng Yu
Methodology: Dong Han, Hongbo Zhang
Writing – original draft: Danyang Zhao, Yu Wang
Writing – review & editing: Qingfeng Li, Dong Han, Hongbo Zhang

Ethics approval and consent to participate

Animal experiments and surgical procedures were approved by Research Ethics Committee of Shanghai Jiagan Biotechnology Co., Ltd (ethics approval number: JGLL20210702) and conducted in accordance with the Guide for Care of Laboratory Animals outlined by the National Ministry of Science.

Consent for publication

Not applicable.

Availability of data

Not applicable.

References

1. Roddy E, DeBaun MR, Daoud-Gray A*, et al.*, 2018, Treatment of critical-sized bone defects: Clinical and tissue engineering perspectives. *Eur J Orthop Surg Traumatol*, 28(3):351–362.

   https://doi.org/10.1007/s00590-017-2063-0

2. Zhao D, Wang Y, Han D, 2016, Periosteal distraction osteogenesis: An effective method for bone regeneration. *Biomed Res Int*, 2016:2075317.

   https://doi.org/10.1155/2016/2075317

3. Bakhshandeh B, Zarrintaj P, Oftadeh M O, *et al.*, 2017, Tissue engineering; strategies, tissues, and biomaterials. *Biotechnol Genet Eng Rev*, 33(2):144-172.

   https://doi.org/10.1080/02648725.2018.1430464.

4. Mercado-Pagan AE, Stahl AM, Shanjani Y*, et al.*, 2015, Vascularization in bone tissue engineering constructs. *Ann Biomed Eng*, 43(3):718–729.

   https://doi.org/10.1007/s10439-015-1253-3

5. Moradi A, Pakizeh M, Ghassemi T, 2021, A review on bovine hydroxyapatite; extraction and characterization. *Biomed Phys Eng Express*, 8(1):2057-1976.

   https://doi.org/10.1088/2057-1976/ac414e

6. Alizadeh-Osgouei M, Li Y, Wen C, 2019, A comprehensive review of biodegradable synthetic polymer-ceramic composites and their manufacture for biomedical applications. *Bioact Mater*, 4(1):22–36.

   https://doi.org/10.1016/j.bioactmat.2018.11.003

7. Fitzgerald R, Bass LM, Goldberg DJ*, et al.*, 2018, Physiochemical characteristics of poly-L-lactic acid (PLLA). *Aesthet Surg J*, 38(suppl_1):S13–S17.

   https://doi.org/10.1093/asj/sjy012

8. Blanpain C, Fuchs E, 2014, Stem cell plasticity. Plasticity of epithelial stem cells in tissue regeneration. *Science*, 344(6189):1242281.

   https://doi.org/10.1126/science.1242281

9. Lin H, Sohn J, Shen H*, et al.*, 2019, Bone marrow mesenchymal stem cells: Aging and tissue engineering applications to enhance bone healing. *Biomaterials*, 203:96–110.

   https://doi.org/10.1016/j.biomaterials.2018.06.026

10. Baldwin JG, Wagner F, Martine LC, *et al.*, 2017, Periosteum tissue engineering in an orthotopic in vivo platform. *Biomaterials*, 121:193–204.

    https://doi.org/10.1016/j.biomaterials.2016.11.016

11. Zhang X, Awad HA, O'Keefe RJ*, et al.*, 2008, A perspective: Engineering periosteum for structural bone graft healing. *Clin Orthop Relat Res*, 466(8):1777–1787.

    https://doi.org/10.1007/s11999-008-0312-6

12. Ferretti C, Mattioli-Belmonte M, 2014, Periosteum derived stem cells for regenerative medicine proposals: Boosting current knowledge. *World J Stem Cells*, 6(3):266–277.

    https://doi.org/10.4252/wjsc.v6.i3.266

13. Li N, Song J, Zhu G*, et al.*, 2016, Periosteum tissue engineering-a review. *Biomater Sci*, 4(11):1554–1561.

    https://doi.org/10.1039/c6bm00481d

14. Lou Y, Wang H, Ye G*, et al.*, 2021, Periosteal tissue engineering: Current developments and perspectives. *Adv Healthc Mater*, 10(12):e2100215.

    https://doi.org/10.1002/adhm.202100215

15. Chen D, Zhang X, He Y*, et al.*, 2012, Co-culturing mesenchymal stem cells from bone marrow and periosteum enhances osteogenesis and neovascularization of tissue-engineered bone. *J Tissue Eng Regen Med*, 6(10):822–832.

https://doi.org/10.1002/term.489

16. Liu Y, Chan JK, Teoh SH, 2015, Review of vascularised bone tissue-engineering strategies with a focus on co-culture systems. *J Tissue Eng Regen Med*, 9(2):85–105.

https://doi.org/10.1002/term.1617

17. Borciani G, Montalbano G, Baldini N*, et al.*, 2020, Co-culture systems of osteoblasts and osteoclasts: Simulating in vitro bone remodeling in regenerative approaches. *Acta Biomater*, 108:22–45.

https://doi.org/10.1016/j.actbio.2020.03.043

18. Mandrycky C, Wang Z, Kim K*, et al.*, 2016, 3D bioprinting for engineering complex tissues. *Biotechnol Adv*, 34(4): 422–434.

https://doi.org/10.1016/j.biotechadv.2015.12.011

19. Murphy SV, Atala A, 2014, 3D bioprinting of tissues and organs. *Nat Biotechnol*, 32(8):773–785.

https://doi.org/10.1038/nbt.2958

20. Yue K, Trujillo-de Santiago G, Alvarez MM*, et al.*, 2015, Synthesis, properties, and biomedical applications of gelatin methacryloyl (GelMA) hydrogels. *Biomaterials*, 73: 254–271.

https://doi.org/10.1016/j.biomaterials.2015.08.045

21. Sun M, Sun X, Wang Z*, et al.*, 2018, Synthesis and properties of gelatin methacryloyl (GelMA) gydrogels and their recent applications in load-bearing tissue. *Polymers (Basel)*, 10(11):1290.

https://doi.org/10.3390/polym10111290

22. Zhao D, Jiang W, Wang Y*, et al.*, 2020, Three-dimensional-printed poly-L-lactic acid scaffolds with different pore sizes influence periosteal distraction osteogenesis of a rabbit skull. *Biomed Res Int*, 2020:7381391.

https://doi.org/10.1155/2020/7381391

23. Debnath S, Yallowitz AR, McCormick J*, et al.*, 2018, Discovery of a periosteal stem cell mediating intramembranous bone formation. *Nature*, 562(7725):133–139.

https://doi.org/10.1038/s41586-018-0554-8

24. Yin J, Yan M, Wang Y*, et al.*, 2018, 3D bioprinting of low-concentration cell-laden gelatin methacrylate (GelMA) bioinks with a two-step cross-linking strategy. *ACS Appl Mater Interfaces*, 10(8):6849–6857.

https://doi.org/10.1021/acsami.7b16059

25. Valtanen RS, Yang YP, Gurtner GC*, et al.*, 2021, Synthetic and bone tissue engineering graft substitutes: What is the future? *Injury*, 52(Suppl 2):S72–S77.

https://doi.org/10.1016/j.injury.2020.07.040

26. Zhang W, Wang N, Yang M*, et al.*, 2022, Periosteum and development of the tissue-engineered periosteum for guided bone regeneration. *J Orthop Translat*, 33:41–54.

https://doi.org/10.1016/j.jot.2022.01.002

27. Hadjidakis DJ, Androulakis, II, 2006, Bone remodeling. *Ann N Y Acad Sci*, 1092:385–396.

https://doi.org/10.1196/annals.1365.035

28. Marx RE, 2007, Bone and bone graft healing. *Oral Maxillofac Surg Clin North Am*, 19(4):455–466, v.

https://doi.org/10.1016/j.coms.2007.07.008

29. Colnot C, 2009, Skeletal cell fate decisions within periosteum and bone marrow during bone regeneration. *J Bone Miner Res*, 24(2):274–282.

https://doi.org/10.1359/jbmr.081003

30. Chehelcheraghi F, Chien S, Bayat M, 2019, Mesenchymal stem cells improve survival in ischemic diabetic random skin flap via increased angiogenesis and VEGF expression. *J Cell Biochem*, 120(10):17491–17499.

https://doi.org/10.1002/jcb.29013

31. Kanno T, Takahashi T, Ariyoshi W*, et al.*, 2005, Tensile mechanical strain up-regulates Runx2 and osteogenic factor expression in human periosteal cells: Implications for distraction osteogenesis. *J Oral Maxillofac Surg*, 63(4):499–504.

https://doi.org/10.1016/j.joms.2004.07.023

32. Veeriah V, Paone R, Chatterjee S*, et al.*, 2019, Osteoblasts regulate angiogenesis in response to mechanical unloading. *Calcif Tissue Int*, 104(3):344–354.

https://doi.org/10.1007/s00223-018-0496-z

33. Tabbaa SM, Horton CO, Jeray KJ*, et al.*, 2014, Role of vascularity for successful bone formation and repair. *Crit Rev Biomed Eng*, 42(3-4):319–348.

https://doi.org/10.1615/critrevbiomedeng.2014011662

34. Dixon DT, Gomillion CT, 2021, Conductive scaffolds for bone tissue engineering: Current state and future outlook. *J Funct Biomater*, 13(1):1.

https://doi.org/10.3390/jfb13010001

35. Elhattab K, Bhaduri SB, Sikder P, 2022, Influence of fused deposition modelling nozzle temperature on the rheology and mechanical properties of 3D printed beta-tricalcium phosphate (TCP)/polylactic acid (PLA) composite. *Polymers (Basel)*, 14(6):1222.

https://doi.org/10.3390/polym14061222

36. Ngo HX, Bai Y, Sha J*, et al.*, 2021, A narrative review of u-HA/PLLA, a bioactive resorbable reconstruction material: Applications in oral and maxillofacial surgery. *Materials (Basel)*, 15(1):150.

https://doi.org/10.3390/ma15010150

37. Hanafusa S, Matsusue Y, Yasunaga T, *et al.*, 1995, Biodegradable plate fixation of rabbit femoral shaft osteotomies. A comparative study. *Clin Orthop Relat Res*, 315(6):262–271.

38. Bigham-Sadegh A, Oryan A, 2015, Selection of animal models for pre-clinical strategies in evaluating the fracture healing, bone graft substitutes and bone tissue regeneration and engineering. *Connect Tissue Res*, 56(3):175–194.

    https://doi.org/10.3109/03008207.2015.1027341

39. Xiao S, Zhao T, Wang J, *et al.*, 2019, Gelatin methacrylate (GelMA)-based hydrogels for cell transplantation: An effective strategy for tissue engineering. *Stem Cell Rev Rep*, 15(5):664–679.

    https://doi.org/10.1007/s12015-019-09893-4

40. Van Den Bulcke AI, Bogdanov B, De Rooze N, *et al.*, 2000, Structural and rheological properties of methacrylamide modified gelatin hydrogels. *Biomacromolecules*, 1(1):31–38.

    https://doi.org/10.1021/bm990017d